Applied Physics Letters

Bright infra-red quantum dot light-emitting diodes through efficient suppressing of electrons

Cite as: Appl. Phys. Lett. **116**, 191103 (2020); https://doi.org/10.1063/5.0005843
Submitted: 26 February 2020 . Accepted: 29 April 2020 . Published Online: 12 May 2020

M. Marus, Y. Xia, H. Zhong, D. Li, S. Ding, U. Turavets, B. Xu, K. Wang, J. Zhang, and X. W. Sun

Applied Physics Letters ARTICLE scitation.org/journal/apl

Bright infra-red quantum dot light-emitting diodes through efficient suppressing of electrons

Cite as: Appl. Phys. Lett. **116**, 191103 (2020); doi: 10.1063/5.0005843
Submitted: 26 February 2020 · Accepted: 29 April 2020 ·
Published Online: 12 May 2020

M. Marus,[1,2] Y. Xia,[3] H. Zhong,[2] D. Li,[2] S. Ding,[1,2] U. Turavets,[2] B. Xu,[1,2] K. Wang,[2] J. Zhang,[3] and X. W. Sun[1,2,a)]

AFFILIATIONS

[1]Shenzhen Planck Innovation Technologies Co. Ltd, Shenzhen 518112, China
[2]Shenzhen Key Laboratory of Advanced Quantum Dot Displays and Lighting, Guangdong Higher Education Key Lab of Advanced Quantum Dot Displays and Lighting, and Department of Electrical and Electronic Engineering, Southern University of Science and Technology (SUSTech), 1088 Xueyuan Avenue, Shenzhen 518055, People's Republic of China
[3]School of Optical and Electronic Information, Huazhong University of Science and Technology, Wuhan 430074, China

[a)]**Author to whom correspondence should be addressed:** sunxw@sustech.mail.cn

ABSTRACT

Colloidal quantum dots are promising materials for near infrared light emitting diodes (NIR QLEDs) owing to the widely tunable wavelength of emitted light, high quantum efficiency, and full integration with solution processing techniques. However, the imbalance of charge carriers in NIR QLEDs greatly limits their performance, which in turn narrows the scope of their application. Here, we propose an approach for improving the brightness and stability of NIR PbS QLEDs through balancing the device current by an ultra-thin inorganic aluminum oxide (Al_2O_3) electron suppressing layer. This modification resulted in a 7.42 W/sr/m^2 peak radiance at 1.3 μm wavelength. Moreover, the halide-capped PbS-based NIR QLEDs remained stable under constant current drive for over 144 h.

Semiconductor colloidal quantum dots (QDs) offer many advantages for near infra-red quantum dot-based light emitting diodes (NIR QLEDs) and lasers thanks to their dimension-dependent emission complemented by an accessible and scalable solution processing technique.[1–4] NIR QLEDs naturally gain interest for bio-diagnostic applications, night-vision devices, fiber-optic communication, and proximity sensing.[5–8] Among the NIR emissive QDs, lead sulfide (PbS) nanocrystals received particular attention owing to high photoluminescent quantum yield (PLQY) in solution, less problematic air stability compared to many other NIR QDs such as lead selenide (PbSe), and convenience of being capped with a variety of organic and inorganic ligands, which, in turn, allows significant tuning of the emitting layer in NIR QLEDs.[4,9–11] However, the performance of NIR QLEDs, including PbS-based ones, significantly lags behind their visible counterparts, coming from relatively poor carrier mobility of the organic ligands and charge imbalance resulting in leakage currents and exciton quenching.[5,12,13] For example, mobility of electrons in zinc oxide (ZnO) based electron-transporting layers (ETLs) far exceeds the mobility of holes in organic hole transport layers (HTLs), which lead to undesirable Auger recombination.[14–16]

To address this shortcoming, several approaches have been proposed in NIR QLEDs including tailoring the interdot distance by organic ligands,[9] using a core-shell structure,[12] and embedding PbS QDs in the perovskite matrix.[13] The inter-dot distance in the quantum dot film can be tuned through different lengths of the ligands, which can assist in balancing the carrier injection and enhancing exciton recombination.[9] The process of charge transport and light emission can be effectively decoupled by the passivating shell in the QLED; furthermore, the shell can mitigate the quenching induced by the ZnO.[12] Embedding the QDs in the mixed-halide perovskite increases the diffusion length and transport of carriers to emitting centers, thereby enhancing radiative recombination in QDs, which enabled 4.9% power conversion efficiency in NIR QLED.[13] Here, we propose an accessible method for improving the performance of PbS-based NIR QLEDs through employing solution-phase mixed halide (iodine and bromide) ligand exchange and through balancing device current with an ultra-thin aluminum oxide (Al_2O_3) electron suppressing layer (ESL). PbS QDs with the PL peak at 1300 nm were synthesized via a recently adopted cationic exchange approach from ZnS nanorods,[17] allowing the enhancement of trap-state control in the QD solids. Moreover, inserting an ultra-thin Al_2O_3 ESL effectively suppresses injection of excess electrons into the emitting layer (EML) and reduces the leakage into a hole-transporting layer (HTL), which further augments the device performance.

According to the published procedures, the untreated highly monodisperse PbS QDs were synthesized by the cation-exchange method from ZnS nanorods.[17] Based on the widely used ligand exchange in solar cells,[18–20] the procedures of solution-phase halide treatment to as-synthesized QDs were as follows: 2.0 mmol lead iodide (PbI_2) and 0.4 mmol lead bromide ($PbBr_2$) were mixed in 10 ml of dimethylformamide (DMF) to form the mixed halide precursor, followed by 5 min sonication at room temperature. Then, 5 ml of oleic acid (OA)-capped QDs (8 mg/ml in octane) were added into the mixed halide solution for ligand exchange. The resulting solution was shaken for 30–60 s until the PbS QDs were transferred from nonpolar octane into the polar DMF at the bottom of the solution completely. After that, we removed the octane layer with the residual organic ligands by washing the QD solutions three more times with octane. Finally, the solution with QDs dispersed in the bottom was centrifuged at 9000 rpm for 5 min and vacuumed for 0.5 h. The resulting PbS-halide powder was dissolved in the mixed solution of DMF and butylamine (BTA) (3:7 in v/v) at 100 mg/ml for the following device fabrication.

The Al_2O_3 electron suppressing layer was deposited on the ZnO electron transport layer through trimethylaluminum (TMAl) as an aluminum precursor and H_2O as an oxygen precursor. When the chamber pressure decreased below 0.4 Pa, the two reactive precursors were delivered sequentially in the vicinity of sample substrates by high purity argon carrier gas followed by a purging process. The gas flow rate was 45 sccm. The single atomic layer deposited (ALD) cycle consisted of a 0.7 s supply of H_2O, a 15 s purge of excess H_2O, and a 0.4 s pulse of TMAl in duration, a 15 s purge of excess TMAl, and any surplus reactants. Temperature of the substrate was kept at 100 °C during the process. The growth rate of Al_2O_3 was about 1.0 Å/cycle and the film thickness was controlled by the number of cycles.

The as-prepared halide capped PbS QDs were used for fabricating NIR QLEDs with inverse configuration.[12] Pre-patterned ITO-coated glass substrates (Youxuan, Inc, China) were cleaned with distilled water, acetone, and isopropanol. The 20 mg/ml ZnO nanoparticles (NPs; Mesolight, Inc.) in ethanol were spin-coated onto the pre-cleaned ITO substrate at 3000 rpm and 1500 acceleration rate for 45 s and then baked at 100 °C for 10 min. The Al_2O_3 layer of different thickness was deposited by the ALD process. A single 47.5 nm thick layer of halide-PbS QDs was spin-cast from the DMF:BTA 3:7 mixed solution at 3500 rpm and 1500 acceleration rate for 60 s. After 5 min drying at 80 °C QD film, 60 nm CBP hole transporting layer (HTL), 3 nm MoO_3 hole injection layer (HIL), and 100 nm Au anode were deposited by thermal evaporation with 0.5, 0.1, and 1 Å/s rates in vacuum ($\sim 5 \times 10^{-6}$ Torr), respectively. Those devices were then sealed by putting another clean glass substrate on top with UV-curing adhesives. The entire device fabrication sequence, except for the ZnO NP layer and the thermal evaporation steps, was performed in a glovebox. Each ITO substrate was patterned with a device area of 4 mm^2.

The performance of QD-based optoelectronic devices is closely related to optimizing QD synthesis, choosing a right ligand exchange strategy and device configuration. The acquisition of excellent quality QDs is first considered, from the perspectives of PLQY, uniform size distribution, and outstanding air stability. Considering the as-synthesized PbS QDs, the exposed crystal faces of the QDs and the ratio of {100}[21] facet to {111}[22] facet vary greatly when increasing the size of these NCs. The {100} facet surface with alternating rows of Pb and S atoms, due to incomplete ligand passivation, is still susceptible to water and oxygen, which introduce unacceptable surface defects.[23] Here, we employ the recently adopted cationic exchange synthesis utilizing ZnS nanorods,[17] which enables PbS QDs with excellent size distribution and strong stability. Additionally, these {100} facets of these PbS QDs were passivated with chloride,[24] giving rise to effective control of trap states. The absorption and PL spectra of the PbS QDs used in this work are shown in Fig. 1(a). The first exciton absorption peak of the QDs in octane solvent lies at 1280 nm and the PLQY reaches around 18%. Figure 1(b) demonstrates the low-magnification transmission electron microscopy (TEM) image of the as-synthesized QDs highlighting their uniform size distribution with an average QD size of around 4.8 nm. There are two key benefits of this synthesis approach which greatly enhance the performance of NIR QLED devices.[17] First, due to *in situ* chloride passivation, the QDs become less sensitive to air in ambient atmosphere and possess fewer trap states in the solid state. Second, ZnS NRs used as precursors allow excellent monodispersity of the PbS QDs and offer better carrier transport in QD films. From the general perspective, this method enables QDs with "clean" surface leading to efficient ligand exchange, stronger electronic coupling, and higher mobility in optoelectronic devices.[17]

In NIR QLEDs, the insulating organic long chain on the surface of QDs will lead to inefficient charge transportation and injection, impeding carrier transport in the emissive layer, so it is indispensable to displace the surface ligand of the as-synthesized QDs before device fabrication. There are a wide range of ligand exchange methods to treat the surface of QDs, which can be generally categorized as solid-state ligand exchange and liquid phase ligand exchange.[25–27] Mostly, layer by layer deposition by solid-state ligand exchange is employed for ligand exchange in NIR QLEDs.[9,28] However, some studies have suggested that this strategy tends to induce uneven energy distribution and cause residual organic matter in the QD films to hinder carrier transportation in optoelectronic devices.[29–31] Therefore, as depicted in Fig. 2(a), we apply solution-phase mixed halide ligands by PbI_2 and $PbBr_2$ to treat the as-synthesized PbS QDs, which enable closely packed QD films with beneficial carrier transport.[18,20,31–33] X-ray photoelectron spectroscopy confirmed that PbS QDs were capped by I and Br ions. As shown in Fig. 2(b), strong binding energy peaks of I 3d at 619.2 eV and 636.6 eV and Br 3D at 619.2 eV and 636.6 eV appeared following the solution-phase halide treatment.

Furthermore, we employed an ultra-thin Al_2O_3 to address the known issue of charge imbalance in inverted QLEDs, which results in leakage currents and exciton quenching due to Auger

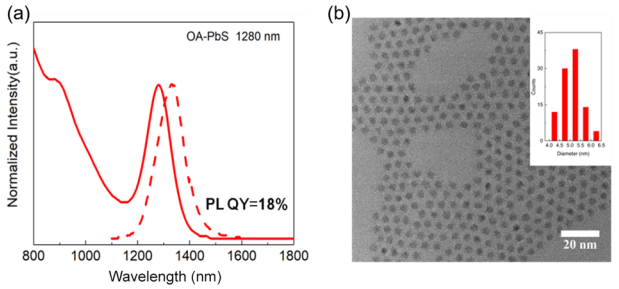

FIG. 1. (a) Absorption and PL spectra of the as-synthesized PbS QDs. (b) TEM of the as-synthesized PbS (1280 nm) QDs; the illustration is a size distribution histogram.

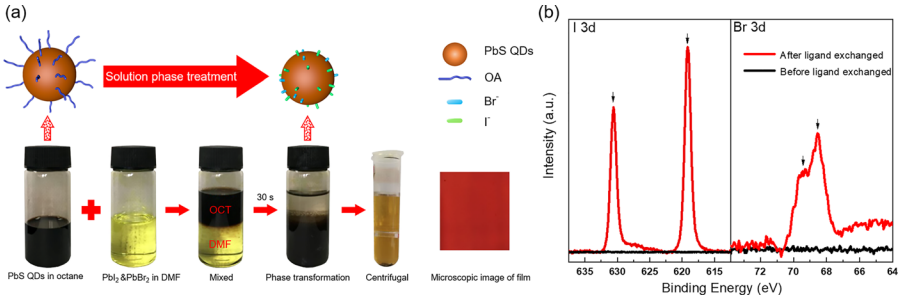

FIG. 2. (a) The ligand exchange procedure to produce solution-phase halide treated QDs. (b) XPS of PbS QD films before and after ligand exchange.

recombination.[25–27,34] Compared to widely used organic electron blocking layers such as poly(methyl methacrylate) (PMMA), Al_2O_3 allows not only precise thickness control and excellent uniformity (up to 1 Å per ALD cycle), but also benefits from being oxygen and moisture insensitive.[35,36] Here, we utilized the ultraviolet photoelectron spectroscopic (UPS) measurement to characterize the electronic structures of ZnO/Al_2O_3 films on indium tin oxide (ITO) glass with thicknesses of Al_2O_3 ESL ranging from 0 to 3.0 nm. Figures 3(a) and 3(b) display the secondary electron cutoff and the valence band onset regions of the samples, respectively. The valence band maximum (VBM) can be calculated according to the following equation VBM = 21.2 – (E_{cutoff} – E_{onset}), where E_{onset} is the valence band onset energy. Hence, the VBM levels of ZnO/Al_2O_3 films on indium tin oxide (ITO) glass with 0, 1.5, and 3.0 nm ESL are measured to be 7.24, 7.21, and 7.07 eV. The UV-visible absorption spectra of all samples illustrated as the plots of $(\alpha h\nu)^2$ vs $h\nu$ are shown in Fig. 3(c), where α is the absorbance coefficient and $h\nu$ is the photoenergy, and the bandgap (E_g) can be able to be from the absorption onset of the linear region. As a result, the conduction band minimum (CBM) values are estimated to be 3.73, 3.70, and 3.58 eV for ZnO/Al_2O_3 films with 0, 1.5, and 3.0 nm ESL, respectively. Hence, as shown in Fig. 4, the increment of Al_2O_3 thickness leads to a higher barrier for the electrons into PbS EML, which reduces the amounts of excess electrons and undesirable energy transfer from excitons to free electrons at the interface of ZnO/QDs. Moreover, an ultra-thin Al_2O_3 layer serves as a perfect inorganic platform for solution processed deposition of PbS-halide QDs thanks to reducing the root-mean square (RMS) surface roughness of the ZnO layer[14,15] and can be utilized for moisture and oxygen protection of the emissive layer of QLEDs.

To evaluate the influence of the Al_2O_3 ESL ranging from 0 to 3.0 nm on the performance of devices, the as-prepared halide capped PbS QDs were used for fabricating NIR QLEDs with inverse configuration as shown in Fig. 5(a). We have chosen the inverse configuration of the NIR QLED as it demonstrated viable efficiency and offers using a highly stable inorganic ZnO layer as a ground for solution processing of QD films without damaging it with solvents.[12] In such a configuration, pre-patterned and cleaned indium tin oxide (ITO), solution processed ZnO nanoparticle layer (30 nm), atomic layer deposited (ALD)

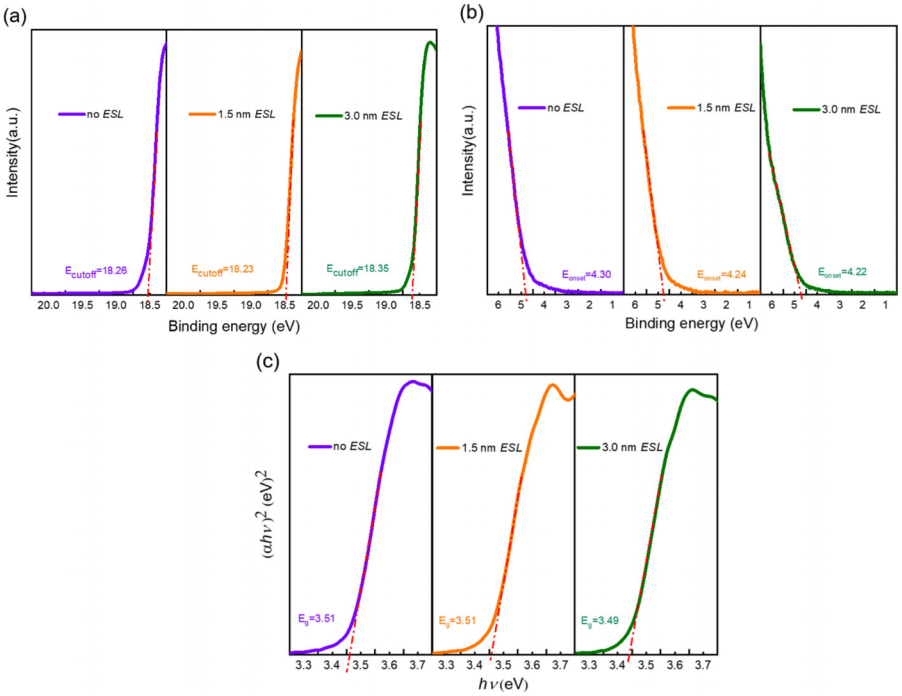

FIG. 3. Ultraviolet photoemission spectroscopy (UPS) measurement of (a) secondary-electron cutoff and (b) valence-band edge regions of ZnO/Al_2O_3 films on indium tin oxide (ITO) glass with thicknesses of Al_2O_3 ESL ranging from 0 to 3.0 nm. (c) $(\alpha h\nu)^2$-$h\nu$ plots converted from the absorption spectra of the samples.

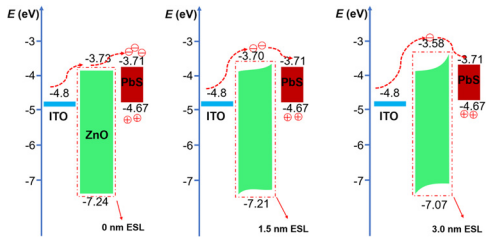

FIG. 4. Energy level diagram of the Al_2O_3-modified ZnO ETL layer depending on the varying Al_2O_3 thickness: 0 nm, 1.5 nm, and 3.0 nm.

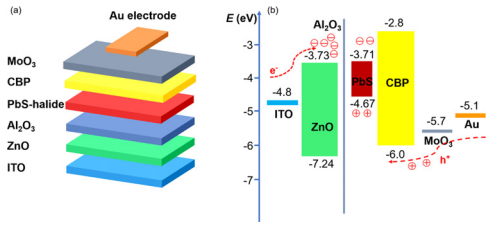

FIG. 5. (a) Device configuration. (b) Energy level diagram of the PbS-halide QLED.

Al_2O_3 (1.5–3.0 nm), thermally evaporated 4,4-bis(carbazole-9-yl) biphenyl (CBP, 60 nm), molybdenum oxide (MoO_3, 4.5 nm), and a gold electrode function as a cathode, an electron transport layer (ETL), an electron suppressing layer, a small-molecule hole transporting layer (HTL), a hole injection layer (HIL), and an anode, respectively, while a PbS-halide based emitting layer (47.5 nm), sandwiched between ZnO and CBP, functions as an emitting layer. An energy level diagram of the PbSe-halide QLED is shown in Fig. 5(b). Among the carrier transport layers, MoO_3 can efficiently enhance the hole injection from the Au anode into the deep highest occupied molecular orbital (HOMO) of CBP. Fig. 6(a) shows the electroluminescence (EL) spectra of PbS-halide QLEDs fabricated with 0 nm (purple), 1.5 nm (orange), and 3.0 nm (green) Al_2O_3 ESLs. Electrical characteristics and voltage-radiance dependence of the NIR QLEDs are shown in Figs. 6(b) and 6(c), respectively. Compared to the reference device with no ESL applied, the current density has been decreased for the device with a 1.5 nm thick Al_2O_3 layer; albeit the effect took place before turn on voltage of the device. After 2.1 V, the current density of the NIR QLED with a 1.5 nm Al_2O_3 layer exceeded the current density of the device without the ESL, which can be caused by significantly earlier turn on and increased recombination current of the balanced device. Radiance measurement suggests the device turn on at 3.5 V, but this comes from the limitation of our measurement setup (high lowest detectable radiance = 0.1 W/sr/m^2). At the same time, the NIR QLED device with a 3.0 nm thick Al_2O_3 layer demonstrated significantly lower current for the whole range of applied voltages. The reference PbS-halide NIR QLED reached a maximum radiance of 2.14 W/sr/m^2, being far surpassed by the device utilizing a 1.5 nm Al_2O_3 ESL, which, in turn, reached 7.42 W/sr/m^2 radiance. Significantly higher brightness of the device with an ESL sandwiched between ZnO ETL and PbS-halide emitter results from reducing the exciton quenching due to Auger recombination via efficient suppression of excessive electrons, i.e., balancing the current.[25–27,34–37] However, further increase in the Al_2O_3 thickness hinders maximum radiance of the NIR QLED as indicated in Fig. 6(c) owing to the increase in the tunneling barrier introduced by this insulating layer.[37] In order to test the electron suppressing effect of Al_2O_3 thin films, we fabricated electron-only devices with configuration ITO/ZnO/Al_2O_3/QDs/Al. Figure 7(a) shows current density–voltage characteristics of the electron-only

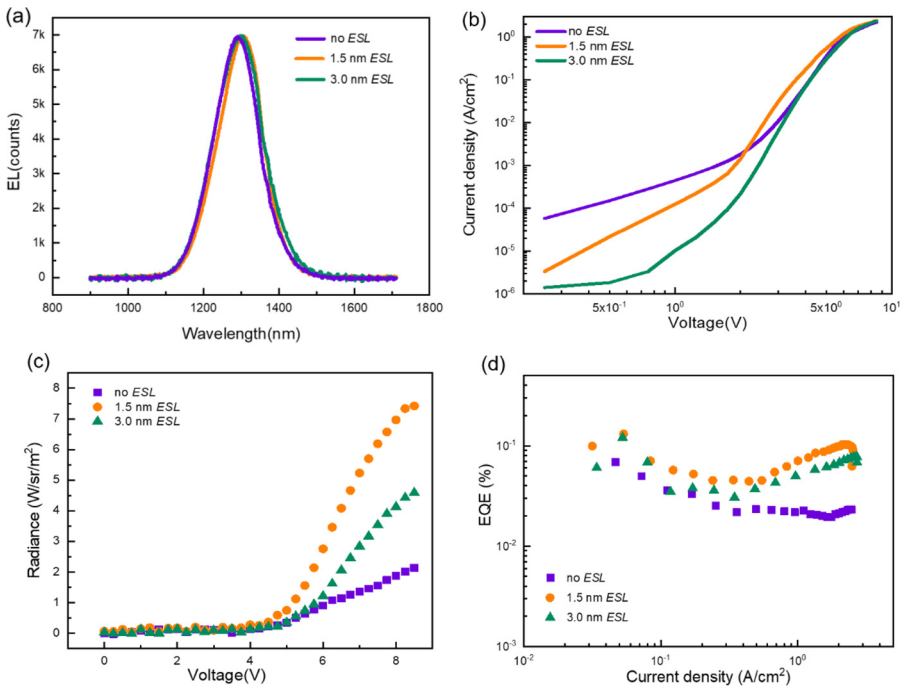

FIG. 6. (a) EL spectra of Pb-halide based NIR QLEDs with 0 (purple), 1.5 (orange), and 3.0 nm (green) Al_2O_3 ESL, respectively. (b) Current density–voltage characteristics of the devices. (c) Radiance–voltage characteristics of the devices. (d) EQE-current density performance of the devices.

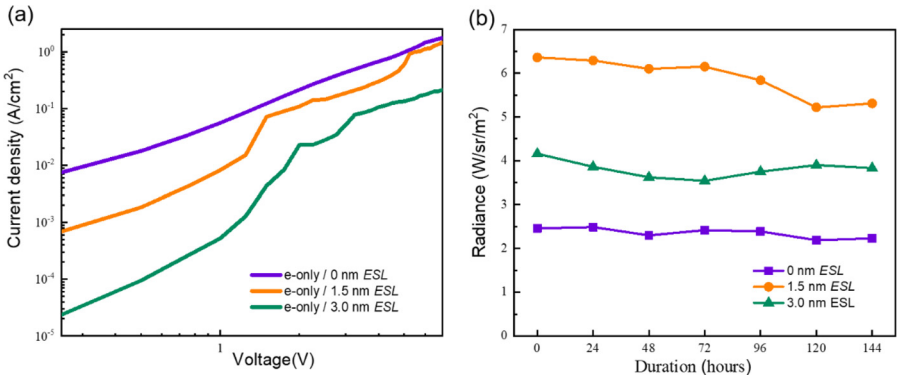

FIG. 7. (a) Current density–voltage characteristics of electron-only devices with varying ESL thickness: 0, 1.5, and 3.0 nm. (b) Peak radiance of NIR QLED control devices with 0, 1.5, and 3.0 nm Al_2O_3 ESL layer measured over 144 hours.

devices with an ESL thickness of 0 nm, 1.5 nm, and 3.0 nm. As expected, the current densities of the devices with 1.5 nm and 3.0 nm thick Al_2O_3 were significantly lower compared to those of the device without ESL. Hence, finding the appropriate thickness of the suppressing layer plays a crucial role in the trade-off between blocking excess electrons to balance the carriers without introducing an overly wide barrier. As shown in Fig. 4(d), the NIR QLED with 1.5 nm Al_2O_3 reached higher efficiency compared to devices with no ESL and 3.0 nm thick ESL—0.13% compared to 0.07 and 0.12%, respectively (limited by the threshold of our measurement setup).

To test the stability of the NIR QLED based on PbS QDs with solid-state mixed halide ligand exchange, we fabricated several additional devices according to the same procedure described in the Experimental section. The results of daily testing over 144 h are shown in Fig. 7(b). The maximum radiance decreased 9.3, 16.5, and 7.9% for devices with 0, 1.5, and 3.0 nm ESL layers, respectively, indicating strong stability of the devices.

In summary, we propose a convenient and effective method of improving the brightness of PbS-based NIR QLEDs through solution-phase halide ligand exchange of QDs combined with balancing the device current by an ultra-thin Al_2O_3 ESL. Owing to these modifications, the PbS-halide QLED reached a maximum radiance of 7.42 W/sr/m^2, which is 3.45 times higher compared to that of the reference device without an ESL. Hence, halide ligand exchange offers effective capping of PbS with short inorganic ligands for densely packed and crack-free QD films with good transport properties, while embedding the Al_2O_3 ESL allows balancing the device current without known drawbacks of using organic insulators. Both techniques can be adopted for making brighter NIR QLEDs for a wide range of potential applications in the areas of communications, bio-diagnostics, night vision, and others.

AUTHOR'S CONTRIBUTION

M.M., Y.X., and H.Z. contributed equally to this work.

X.W.S. would like to acknowledge the support from the National Key Research and Development Program of China administrated by the Ministry of Science and Technology of China (No. 2016YFB0401702); National Natural Science Foundation of China (Nos. 61674074, 61405089, and 61974052), Shenzhen Peacock Team Project (No. KQTD2016030111203005); Shenzhen Innovation Project (Nos. JCYJ20160301113356947 and JCYJ20160301113537474); Shenzhen Key Lab of Advanced Quantum Dot Displays and Lighting, Guangdong Higher Education Key Lab of Advanced Quantum Dot Displays and Lighting, and High Level University of Guangdong Province.

DATA AVAILABILITY

The data that support the findings of this study are available from the corresponding author upon reasonable request.

REFERENCES

[1]E. H. Sargent, Adv. Mater. **17**(5), 515 (2005).
[2]J. S. Steckel, S. Coe-Sullivan, V. Bulović, and M. G. Bawendi, Adv. Mater. **15**(21), 1862 (2003).
[3]M. Grundmann, A. Weber, K. Goede, V. M. Ustinov, A. E. Zhukov, N. N. Ledentsov, P. S. Kop'ev, and Z. I. Alferov, Appl. Phys. Lett. **77**(1), 4 (2000).
[4]F. W. Wise, Acc. Chem. Res. **33**(11), 773 (2000).
[5]N. D. Bronstein, M. S. Martinez, D. M. Kroupa, M. Voros, H. Lu, N. P. Brawand, A. J. Nozik, A. Sellinger, G. Galli, and M. C. Beard, ACS Nano **13**(4), 3839 (2019).
[6]G. Konstantatos, I. Howard, A. Fischer, S. Hoogland, J. Clifford, E. Klem, L. Levina, and E. H. Sargent, Nature **442**(7099), 180 (2006).
[7]T. Rauch, M. Böberl, S. F. Tedde, J. Fürst, M. V. Kovalenko, G. Hesser, U. Lemmer, W. Heiss, and O. Hayden, Nat. Photonics **3**(6), 332 (2009).
[8]A. D. Smith, M. R. F. Siggel-King, G. M. Holder, A. Cricenti, M. Luce, P. Harrison, D. S. Martin, M. Surman, T. Craig, and S. D. Barrett, Appl. Phys. Lett. **102**(5), 053701 (2013).
[9]L. Sun, J. J. Choi, D. Stachnik, A. C. Bartnik, B.-R. Hyun, G. G. Malliaras, T. Hanrath, and F. W. Wise, Nat. Nanotechnol. **7**(6), 369 (2012).
[10]D. M. Kroupa, N. C. Anderson, C. V. Castaneda, A. J. Nozik, and M. C. Beard, Chem. Commun. **52**(96), 13893 (2016).
[11]M. A. Hines and G. D. Scholes, Adv. Mater. **15**(21), 1844 (2003).
[12]G. J. Supran, K. W. Song, G. W. Hwang, R. E. Correa, J. Scherer, E. A. Dauler, Y. Shirasaki, M. G. Bawendi, and V. Bulović, Adv. Mater. **27**(8), 1437 (2015).
[13]X. Gong, Z. Yang, G. Walters, R. Comin, Z. Ning, E. Beauregard, V. Adinolfi, O. Voznyy, and E. H. Sargent, Nat. Photonics **10**(4), 253 (2016).
[14]H. Jin, H. Moon, W. Lee, H. Hwangbo, S. H. Yong, H. K. Chung, and H. Chae, RSC Adv. **9**(21), 11634 (2019).
[15]Z. Li, Vacuum **137**, 38 (2017).
[16]X. Dai, Z. Zhang, Y. Jin, Y. Niu, H. Cao, X. Liang, L. Chen, J. Wang, and X. Peng, Nature **515**(7525), 96 (2014).
[17]Y. Xia, S. Liu, K. Wang, X. Yang, L. Lian, Z. Zhang, J. He, G. Liang, S. Wang, and M. Tan, Adv. Funct. Mater. **30**, 1907379 (2020).
[18]X. Lan, O. Voznyy, F. P. García de Arquer, M. Liu, J. Xu, A. H. Proppe, G. Walters, F. Fan, H. Tan, and M. Liu, Nano Lett. **16**(7), 4630 (2016).
[19]J. Kim, O. Ouellette, O. Voznyy, M. Wei, J. Choi, M.-J. Choi, J. W. Jo, S.-W. Baek, J. Fan, and M. I. Saidaminov, Adv. Mater. **30**(45), 1803830 (2018).
[20]J. Choi, J. W. Jo, F. P. G. de Arquer, Y.-B. Zhao, B. Sun, J. Kim, M.-J. Choi, S.-W. Baek, A. H. Proppe, and A. Seifitokaldani, Adv. Mater. **30**(29), 1801720 (2018).

[21]K. R. Choudhury, D. W. Song, and F. So, Org. Electron. **11**(1), 23 (2010).
[22]R. W. Crisp, D. M. Kroupa, A. R. Marshall, E. M. Miller, J. Zhang, M. C. Beard, and J. M. Luther, Sci. Rep. **5**, 9945 (2015).
[23]Y. Kim, F. Che, J. W. Jo, J. Choi, F. P. García de Arquer, O. Voznyy, B. Sun, J. Kim, M.-J. Choi, and R. Quintero-Bermudez, Adv. Mater. **31**(17), 1805580 (2019).
[24]J. Y. Woo, J.-H. Ko, J. H. Song, K. Kim, H. Choi, Y.-H. Kim, D. C. Lee, and S. Jeong, J. Am. Chem. Soc. **136**(25), 8883 (2014).
[25]D. Bederak, D. M. Balazs, N. V. Sukharevska, A. G. Shulga, M. Abdu-Aguye, D. N. Dirin, M. V. Kovalenko, and M. A. Loi, ACS Appl. Nano Mater. **1**(12), 6882 (2018).
[26]D. M. Balazs, D. N. Dirin, H.-H. Fang, L. Protesescu, G. H. ten Brink, B. J. Kooi, M. V. Kovalenko, and M. A. Loi, ACS Nano **9**(12), 11951 (2015).
[27]Z. Zhang, J. Yang, X. Wen, L. Yuan, S. Shrestha, J. A. Stride, G. J. Conibeer, R. J. Patterson, and S. Huang, J. Phys. Chem. C **119**(42), 24149 (2015).
[28]Z. Yang, O. Voznyy, M. Liu, M. Yuan, A. H. Ip, O. S. Ahmed, L. Levina, S. Kinge, S. Hoogland, and E. H. Sargent, ACS Nano **9**(12), 12327 (2015).
[29]H. Beygi, S. A. Sajjadi, A. Babakhani, J. F. Young, and F. C. van Veggel, Appl. Surf. Sci. **459**, 562 (2018).
[30]H. Aqoma and S.-Y. Jang, Energy Environ. Sci. **11**(6), 1603 (2018).
[31]H. Aqoma, M. Al Mubarok, W. T. Hadmojo, E.-H. Lee, T.-W. Kim, T. K. Ahn, S.-H. Oh, and S.-Y. Jang, Adv. Mater. **29**(19), 1605756 (2017).
[32]M. Liu, O. Voznyy, R. Sabatini, F. P. G. de Arquer, R. Munir, A. H. Balawi, X. Lan, F. Fan, G. Walters, and A. R. Kirmani, Nat. Mater. **16**(2), 258 (2017).
[33]G. H. Carey, L. Levina, R. Comin, O. Voznyy, and E. H. Sargent, Adv. Mater. **27**(21), 3325 (2015).
[34]H.-T. Vu, C.-Y. Huang, H.-C. Yu, and Y.-K. Su, Org. Electron. **63**, 349 (2018).
[35]L. Shi, T. L. Young, J. Kim, Y. Sheng, L. Wang, Y. Chen, Z. Feng, M. J. Keevers, X. Hao, and P. J. Verlinden, ACS Appl. Mater. Interfaces **9**(30), 25073 (2017).
[36]J. Pan, J. Chen, Q. Huang, L. Wang, and W. Lei, RSC Adv. **7**(69), 43366 (2017).
[37]H.-Y. Li, Y.-F. Liu, Y. Duan, Y.-Q. Yang, and Y.-N. Lu, Materials **8**(2), 600 (2015).